Journal of Molecular Modeling (2020) 26: 131
https://doi.org/10.1007/s00894-020-04405-5

ORIGINAL PAPER

A combined experimental and DFT/TD-DFT studies on the electronic structure, structural and optical properties of quinoline derivatives

Mustafa Kurban[1] · Tevfik Raci Sertbakan[2] · Bayram Gündüz[3]

Received: 29 February 2020 / Accepted: 28 April 2020 / Published online: 11 May 2020

Abstract

In this work, the structural, electronic, and optical features of quinoline derivatives were carried out by experiment and density functional theory (DFT). Our results show that a change in the substitution position of methyl group (CH_3) gives rise to a decrease in the bandgap of quinoline derivatives from 2.75 to 2.50 eV for 2-Chloro-5,7-dimethylquinoline-3-carboxaldehyde (C7DMQCA) and 2-Chloro-5,7-dimethylquinoline-3-carboxaldehyde (C8DMQCA), respectively. From dipole moment, the C7DMQCA has stronger intermolecular interaction which is comparable with the bandgap energies. The absorbance maxima are found between 313 nm (3.96 eV) and 365 nm (3.39 eV) for C7DMQCA and C8DMQCA. The refractive index and optical conductivity of the C7DMQCA are found to be higher than that of the C8DMQCA. Besides, the transmittance, angle of incidence and refraction, and $(\alpha h\vartheta)^2$curves were investigated in detail. Theoretical predictions are also compatible with experimental findings. The study shows the C7DMQCA has desirable properties such as lower optical bandgap, higher refractive index, and optical conductivity than the C8DMQCA.

Keywords Quinoline derivatives · Optical parameters · Bandgap · Absorbance · TD-DFT

Introduction

In recent years, the organic semiconductor materials (OSM) have found use in plenty of areas such as solar cells [1–5], light-emitting diodes (LEDs) [6], photodetectors [7], and sensors [8–13]. Organic small molecules, which are a class of OSM, are low molecular weight organic compounds and they have been received increasing interest because of their excellent optoelectronic features which provide high-quality chain-aligned materials [14–16]. Among the small molecules, quinoline is a heterocyclic aromatic organic structure and it is described by a double-ring structure including a benzene ring [17]. On the other hand, the derivations of quinoline are especially used in pharmacology [18–21] and in optoelectronic applications such as the optical switches, sensors, and inorganic chemistry [22, 23] due to their diverse notable features. Besides, there are many investigations on the quinoline and its derivatives to explore their electronic structures [24] and contribution to organic electronics [25–27].

To our knowledge, there is no information about the characteristic properties of two quinoline derivatives 2-Chloro-5,7-dimethylquinoline-3-carboxaldehyde and 2-Chloro-5,8-dimethylquinoline-3-carboxaldehyde. Thus, the purpose of this study is to explore the electronic structure, structural and optical features of the molecules, and also compare the effects of a change in the substitution position of methyl group (CH_3) on the studied properties of the molecules. The experimental findings have also been confronted with that of density functional theory (DFT) calculations for the first time. We first performed some functionals and suitable basis sets to get compatible results with the experiment. The HOMO, LUMO, and HOMO/LUMO gap (E_g) energies, IR and Raman intensity, the density of state (DOS)-optimized bond distances and the lowest frequency vibration modes, and dipole moments were calculated by DFT. The radial distribution functions (RDFs) are also figured out based on the DFT optimized geometry. Using time-dependent (TD)-DFT technique, the predicted absorption of photoexcitations and the optical energy gap have

✉ Mustafa Kurban
mkurbanphys@gmail.com

[1] Department of Electronics and Automation, Kırşehir Ahi Evran University, 40100 Kırşehir, Turkey

[2] Department of Physics, Kırşehir Ahi Evran University, 40100 Kırşehir, Turkey

[3] Department of Science Education, Muş Alparslan University, 49250 Muş, Turkey

been calculated and compared with measured results. The refractive indices (n), transmittance, the angle of incidence and refraction, the $(\alpha h\vartheta)^2$curves versus photon energy (E), and the optical conductivity were measured and discussed in detail.

Experimental details

We purchased the 2-Chloro-5,7-dimethylquinoline-3-carboxaldehyde (C7DMQCA) and 2-Chloro-5,8-dimethylquinoline-3-carboxaldehyde (C8DMQCA) and dichloromethane (DCM) solvent from Sigma–Aldrich Co. We prepared the solutions of the C7DMQCA and C8DMQCA dissolved in DCM solvent and for 2.8 mM concentration. We arranged the amounts of the C7DMQCA and C8DMQCA with an AND-GR-200 series analytical balance. The arranged amounts of the 1 and 2 materials were dissolved in DCM solvent using a digital vortex mixer (Four E's Scientific Co., Ltd.). Then, we recorded the UV-Vis spectra of the C7DMQCA and C8DMQCA with a UV-1800 spectrophotometer (Shimadzu, Japan) at the range of 190–1100 nm.

Computational details

The optimized structures, which are local minima on the potential energy surface, were obtained by DFT [28]. To get reliable results from our calculations, we tested BP86 and B3LYP functionals with TZVP and 6-311G(d,p) basis sets [29–31]. Using the optimized geometry, the absorbance spectra at CAM-B3LYP/6–311 G(d,p) were performed using TD-DFT which is a theoretical approach to the time-dependent electronic many-body problem, which is widely used for calculating electronic excitation energies [32] because the B3LYP functional actually underestimates excited-state energies [33, 34]. The calculations have been performed in the GAUSSIAN09 package [35].

Results and discussion

Structural evaluation, IR and Raman spectra, RDF and dipole moment

The optimized geometries of two quinoline derivatives, which are plotted by GaussView 5.0 [36], are shown in Fig. 1. The lowest vibrational spectra show that the structures are located stationary points on the potential energy surface. The lowest frequency vibration modes of the ground state in DCM were predicted as 46.2852 and 45.7205 cm^{-1}, for C7DMQCA and C8DMQCA, respectively. The total energies were found to be −1053.68975 and − 1053.68996 au for C7DMQCA and

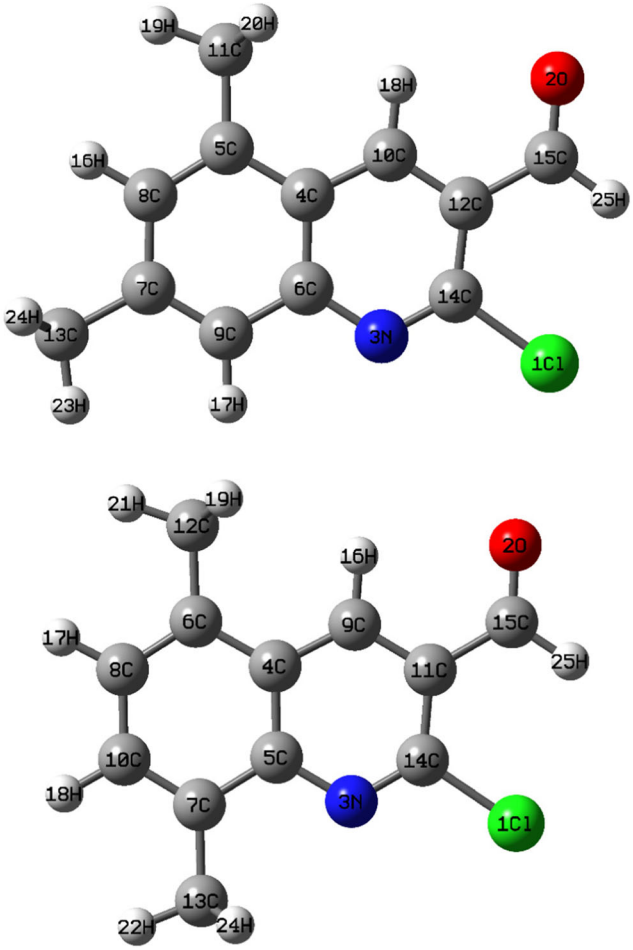

Fig. 1 Optimized ground state geometries of the C7DMQCA (up) and C8DMQCA (down) calculated by BP86/6-311-G(d, p)

C8DMQCA in DCM. Therefore, our results show that the C8DMQCA is more stable than C7DMQCA and they are optimized in C_1 symmetry form. The IR and Raman spectra were also analyzed in detail and indicated in Fig. 2a, b. From Fig. 2a, the IR spectra exhibit the peaks at 2885 (alkyl C-H stretch), 2965, 3050, and 3108 cm^{-1} (C-H bending vibration), at 1680 cm^{-1} (amide C=O stretch and alkenyl C=H stretch), at 1565 cm^{-1} (aromatic C=C bending), at 760 cm^{-1} (aromatic C-H bending), 1449 and 1470 cm^{-1} (C-C stretch (in ring), and C-H bending vibration) and 689, 760 and 813 cm^{-1} (the C-H bending bands). Otherwise, from Fig. 3b, the Raman spectra show the peaks at 2885 cm^{-1} (C-H bending vibration) at 2965 cm^{-1} (C-H_3 stretching), at 3102 cm^{-1} (H bonded CH (in ring)), at 1552 cm^{-1} (aromatic C=C bending), at 1680 cm^{-1} (C=O groups).

The radial distribution function (RDF) is related to the probability of finding a particle in the distance from another particle. It was analyzed for pair separation distance in the C7DMQCA (see Fig. 3). The behavior of RDF is almost the same, so we only compared the experimental and theoretical results for the C7DMQCA. From Fig. 3, the measured RDF is

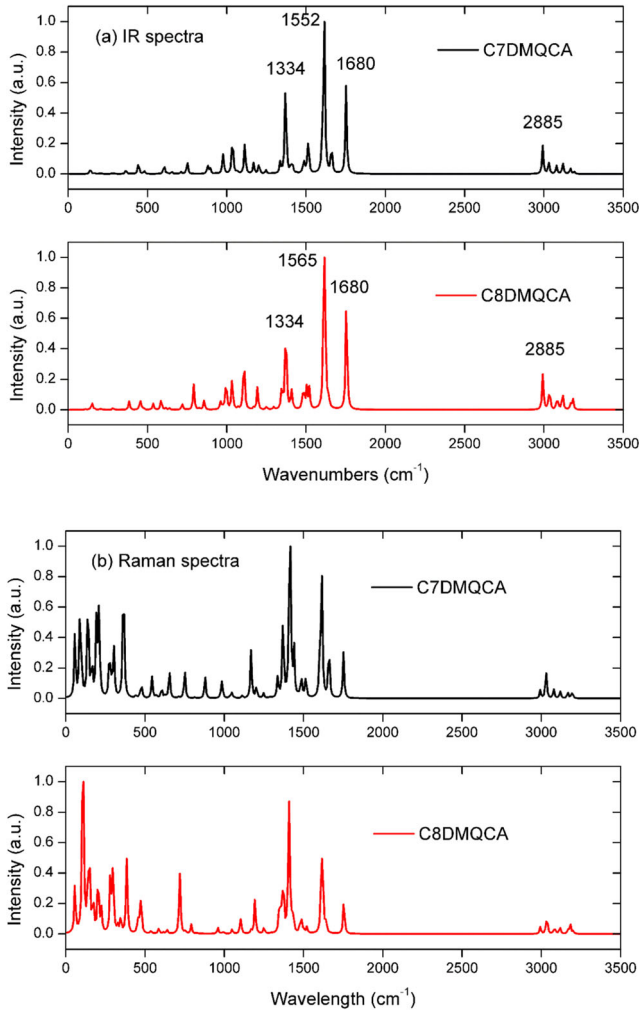

Fig. 2 (**a**) IR and (**b**) Raman spectra of the C7DMQCA and C8DMQCA calculated by BP86/6-311-G(d, p)

narrower and higher than the predicted. The small distributions indicate H-H interactions with C-H bending. The large distributions of RDF show C-N and C-H interactions. When all binary interactions are considered, C-N binary interaction is stronger than that of the others.

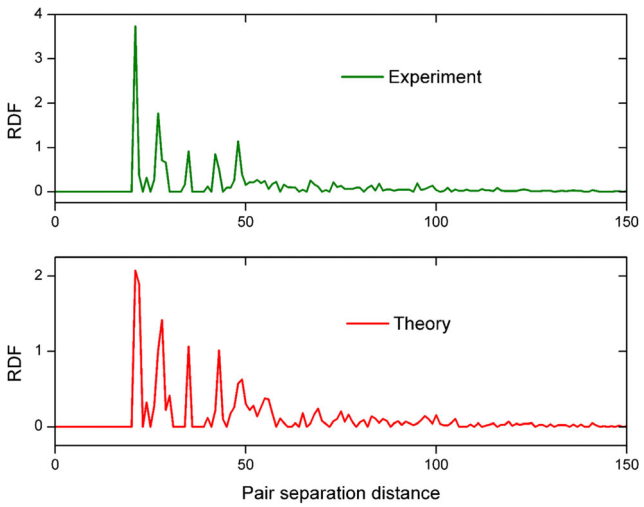

Fig. 3 The measured and calculated radial distribution functions (RDFs) of the C7DMQCA organic molecule

The dipole moment (D_M) is a measure of the charge distribution in a molecule. This occurs when one atom is more electronegative than another. It is well known that electronegativity is a measure of the ability of an atom to attract the electrons. On the other hand, the distance between the charge separation is also a factor into the size of the dipole moment. Our results show that the components of D_M along the x-axis (−5.2978 Debye), y-axis (1.8868 Debye), and z-axis (1.8971) for C7DMQCA give rise to a large charge separation along negative x-direction. Thus, C7DMQCA (5.95 Debye) has a larger D_M favoring electrostatic attractions than that of C8DMQCA (5.02 Debye), which is compatible with the bandgap energies due to the lowest bandgap energy of C8DMQCA in DCM, thus electrons easily transfer from HOMO to LUMO.

Absorbance and transmittance properties

Absorbance spectra of C7DMQCA and C8DMQCA solutions in DCM solvent at 120 μM are depicted in Fig. 4a. From Fig. 4a, the C7DMQCA and C8DMQCA exhibit the absorption maxima at 264 nm (4.69 eV) and 267 nm (4.64 eV) corresponding to the near-ultraviolet (NUV) region in DCM solutions. The C7DMQCA and C8DMQCA also indicate the peaks at 316 nm (3.92 eV) and 326 nm (3.80 eV) which corresponds to the visible (V) region in DCM solvent. We also calculated absorbance spectra using TD-DFT calculations which were exhibited in Fig. 4b. The B3LYP optimized geometry was used to calculate absorbance spectra based on the CAM-B3LYP functional, because DFT/B3LYP(opt) + TD-DFT/CAM-B3LYP gives reasonable results with experiment [33, 34, 37]. The maximum peaks obtained from TD-DFT for the C7DMQCA and C8DMQCA is 262 nm (4.73 eV) and 268 nm (4.62 eV), respectively. The wavelengths with the lowest energy are 313 nm (3.96 eV) and 365 nm (3.39 eV), respectively. Considering the measured absorbance spectra, we can also conclude that the predicted absorbance spectra were found to be excellent compatible with experiment.

Transmittance (T) gives significant characteristics for optical properties. Figures 4a, b also shows T spectra of the C7DMQCA and C8DMQCA. The T value of two quinoline derivatives increases after 280 nm and then decreases up to almost 320 nm where the peaks for two derivatives sharply raise up to 420 nm, and finally, the peaks are found to be constant.

We measured the absorbance band edges ($E_{\text{Abs-be}}$) of two quinoline derivatives using the maximum peaks of the relation of dT/dλ based on wavelength (λ) (see Fig. 5). The $E_{\text{Abs-be}}$ was found to be 2.904 and 3.092 eV for the C7DMQCA and

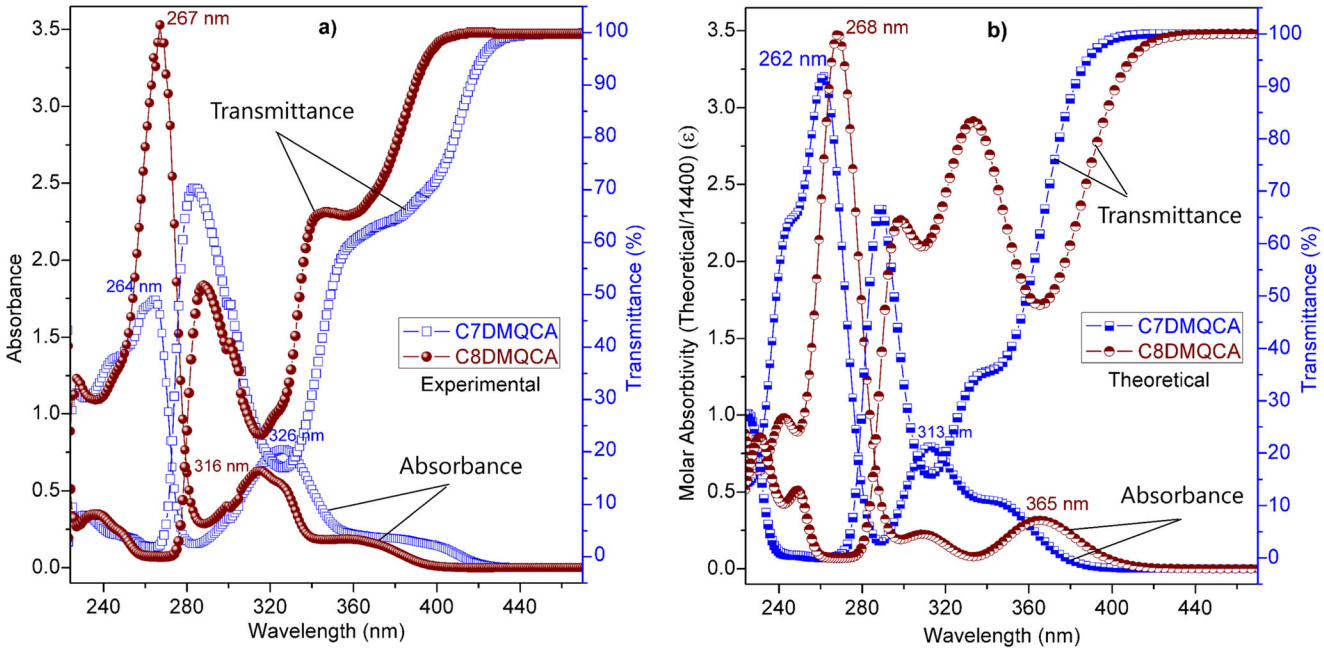

Fig. 4 **a** The experimental absorbance and transmittance spectra. **b** Theoretical absorptivity and transmittance spectra of the C7DMQCA and C8DMQCA

C8DMQCA, respectively. The energy difference between quinoline derivatives is almost 0.2 eV.

The bandgap energy, refractive index, conductivity, incidence, and refractive angles

The bandgap of the organic semiconductors is important to research their electronic and optical features. The optical bandgap (E_{og}) can be estimated from Tauc model given by [38].

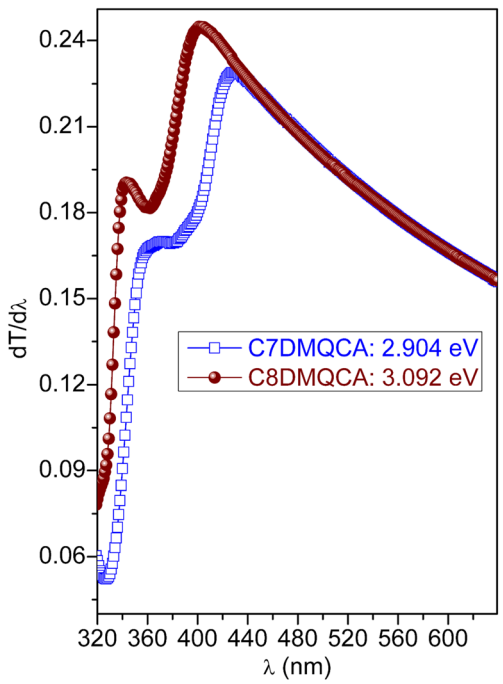

Fig. 5 The $dT/d\lambda$ plots vs. λ of the C7DMQCA and C8DMQCA

$$\alpha(h\vartheta) = A\left(E - E_{og}\right)^{m} \quad (1)$$

where α, $h\vartheta$ (and E), and A are the absorption coefficient, the photon energy, and a constant, respectively and m determines the type of the optical transitions. The m is important to determine the type of transitions because the bandgap can be either direct or indirect. If the m is ½, it is called a direct bandgap, if it is 1, it is called an indirect bandgap. In our study, we found m as ½ for quinoline derivatives, which corresponds to the allowed direct bandgap. We plotted the $(\alpha h\vartheta)^2$ curves in terms of energy (E) to examine bandgap morphology (see Fig. 6). Extrapolating the linear plot to $(\alpha h\vartheta)^2 = 0$, the E_{og} energies were measured as 2.93 eV and 3.12 eV for the C7DMQCA and C8DMQCA, respectively. From the results obtained, the charge transfer mobility in the C7DMQCA is smaller than that in the C8DMQCA organic molecules. This means that the C7DMQCA needs less excitation energy. When it comes to the energy gap, the quinoline derivatives are close to V region. We also performed DFT calculations to figure out the HOMO, LUMO, and electronic bandgap energies (E_{eg}). In this regard, we have tested some functionals (B3LYP and BP86) and basis sets (6-311G(d,p) and TZVP). We made four different benchmarks (B3LYP/6-311G(d,p), B3LYP/TZVP, BP86/6-311G(d,p), and BP86/TZVP) in total to get reasonable results with experimental data. The predicted HOMO, LUMO, and E_{eg} energies were tabulated in Table 1. From Table 1, B3LYP functional underestimate the excitation energies of the

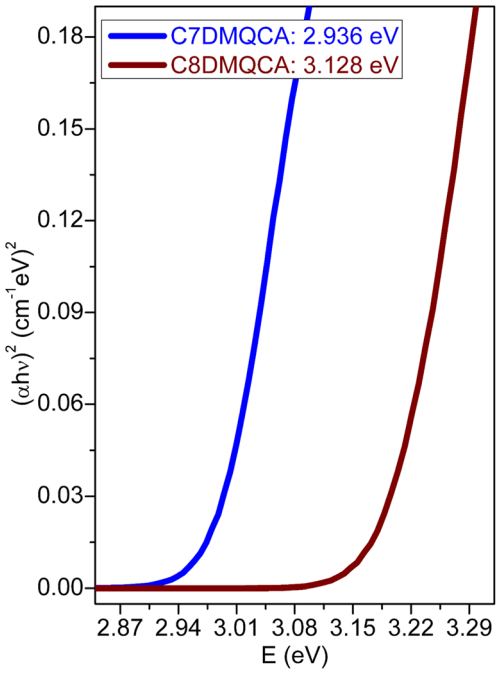

Fig. 6 The $(\alpha hv)^2$ vs photon energy of the C7DMQCA and C8DMQCA

quinoline derivatives and the BP86/6-311G(d,p) level gives compatible results with experiment (see Table 1). Thus, we used this level in the DFT calculations. We perform the density of states (DOS) spectrum obtained Mulliken population analysis to get detailed information on electronic states of the C7DMQCA and C8DMQCA compounds (see Fig. 7). The HOMO and LUMO energies of the C7DMQCA were found to be −6.16 eV and − 3.43 eV, respectively. Furthermore, the HOMO and LUMO energies of the C8DMQCA were predicted as −6.01 eV and − 3.47 eV, respectively. The corresponding E_{eg} energies were found as 2.73 eV and 2.54 eV for the C7DMQCA and C8DMQCA. The illustration of the HOMO, LUMO, and E_{eg} was indicated in Fig. 7 in detail.

Table 1 The HOMO, LUMO, and the bandgap energies (eV) of the quinoline derivatives in DCM solvent

Energy	B3LYP		BP86		
	6-11G(d,p)	TZVP	6-311G(d,p)	TZVP	Exp.
		C7DMQCA			
HOMO	6.754	6.713	6.165	3.502	
LUMO	2.618	2.423	3.432	6.200	
Eg	4.135	4.290	2.733	2.698	2.936
		C8DMQCA			
HOMO	6.608	6.649	6.017	6.045	
LUMO	2.650	2.747	3.476	3.545	
Eg	3..958	3.901	2.541	2.500	3.128

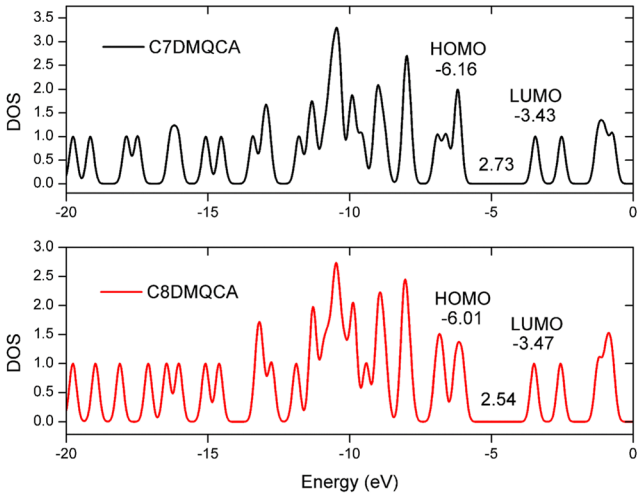

Fig. 7 The density of state (DOS) spectrum of the C7DMQCA and C8DMQCA obtained Mulliken population analysis

The refractive index (n) is a significant parameter in organic electronics because it is an indicator of how different frequencies and wavelengths of light propagate through transparent materials. The n can be defined in terms of reflectance (R) and is calculated from the following equation [39]:

$$n = \left\{ \sqrt{\frac{4R}{(R-1)^2} - k^2} - \frac{R+1}{R-1} \right\} \quad (2)$$

where $k = \alpha\lambda/4\pi$. The n values were examined in terms of angular frequency (ω) and different relations (Hervé-Vandamme, Kumar-Singh, Moss, Ravindra, and Reddy) [40] based on the gap energy (see Fig. 8). From Fig. 8, the n values based on the ω display a normal dispersion behavior in the regions connected with the increase of the n vs. ω curves together. High n materials are progressively dominant in optoelectronics. Herein, the n values of the C7DMQCA are found to be higher than that of the C8DMQCA. Using different relations, we found that the n value obtained from Reddy relation is higher than the other relations, while Ravindra relation is the smallest n value.

Incidence angle (Φ_1) and refraction angle (Φ_2) play a role on the operation of the optical and optoelectronic devices. Especially, the light absorption efficiency of the photovoltaics significantly depends on the Φ_1 angle [41]. We calculated the Φ_1 values using the following equation [39]:

$$\Phi_1 = tan^{-1}\left(\frac{n_2}{n_1}\right) \quad (3)$$

where n_1 and n_2 are the refractive index of the medium and material, respectively. We calculated also the Φ_2 values from Snell's law [42],

$$\Phi_2 = sin^{-1}\left(\frac{n_1}{n_2}\sin\Phi_1\right) \quad (4)$$

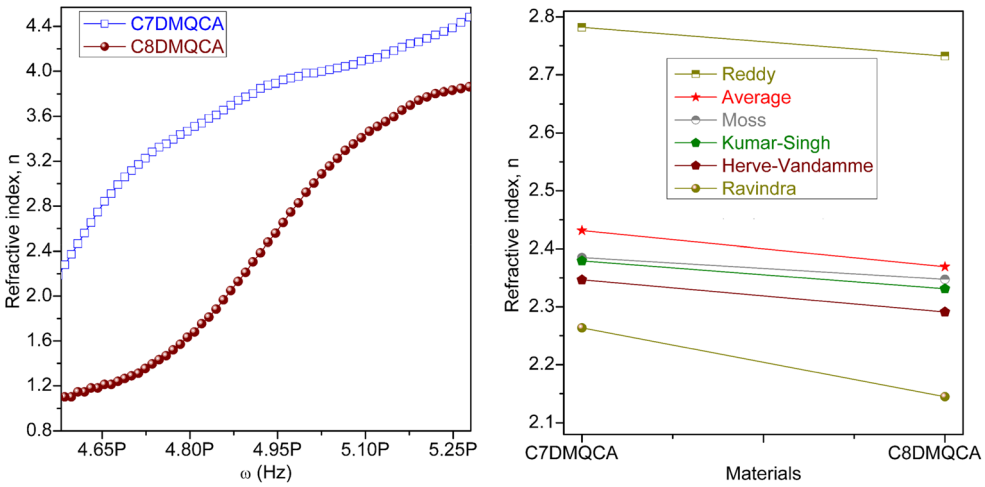

Fig. 8 The refractive index (n) curves of the C7DMQCA and C8DMQCA in terms of angular frequency and different relations

The Φ_1 and Φ_2 plots vs. E of the C7DMQCA and C8DMQCA was indicated in Fig. 9. The Φ_1 and Φ_2 angles of the quinoline derivatives are almost constant up to almost 270 nm (4.59 eV), after that, the angles increase, where the incidence angle values are small differences due to the substitution position of methyl group (CH_3) to the ring. For example, the Φ_2 angle of the C7DMQCA and C8DMQCA increase at almost 330 nm (3.75 eV) and 350 nm (3.45 eV), respectively. Moreover, the incidence angles are higher than the refraction angles.

The optical conductivity (σ) is significant in organic electronic applications because it conveniently gives the optical response of material and is given by the relation [43].

$$\sigma = \frac{\alpha n c}{4\pi} \tag{5}$$

where c, α, and n are the velocity of light, absorption coefficient refractive index, respectively. The σ of the quinoline derivatives is in the range of 10^{11} S^{-1}. Figure 10 indicates the plot of σ in terms of photon energy. The σ was found to increase sharply after 4.2 and 4.3 eV for the C8DMQCA and C7DMQCA, respectively. The reason of these increases is a sharp increase in the absorption coefficient. The σ of the C7DMQCA is higher than that of the C8DMQCA, and the maxima of the peak for the C7DMQCA is at 4.73 eV, while that of the C8DMQCA is at 4.63 eV. The results obtained are compatible with the optical band energy.

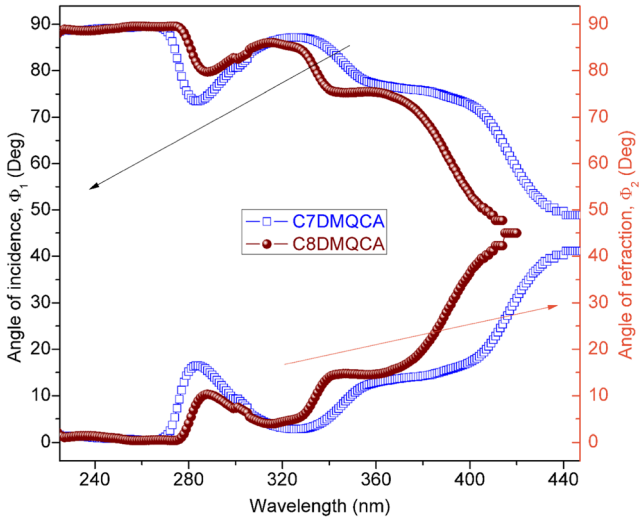

Fig. 9 The Φ_1 and Φ_2 plot vs. E of the solutions of the C7DMQCA and C8DMQCA

Conclusions

The electronic structure, structural and optical features of the quinoline derivatives have been analyzed using the solution technique and DFT/TD-DFT method. The performance of B3LYP and BP86 functionals with 6-311G(d,p) and TZVP was tested for the quinoline derivatives. Comparing with experimental data, the B3LYP functional underestimates excited-state energies, while CAM-B3LYP functional gives

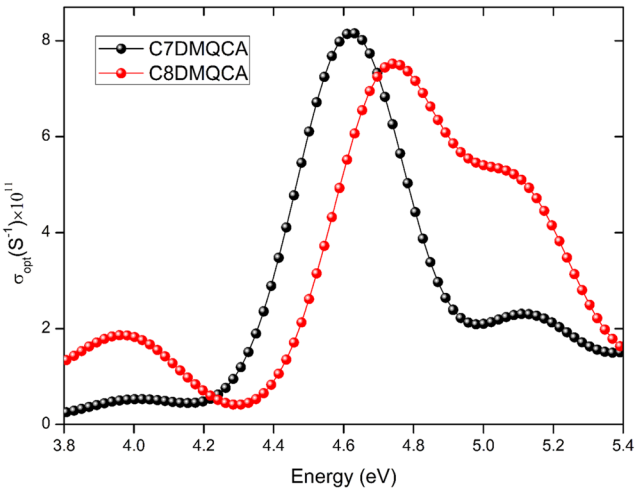

Fig. 10 The optical conductivity curves versus photon energy of the C7DMQCA and C8DMQCA

better results for the absorbance of photoexcitations. Our results show that the geometries of the quinoline derivatives are optimized in the C_1 configuration. Due to the substitution position of methyl group (CH_3), all electronic and optical properties are found to be different. Depending on the total energy and lowest vibrational frequency, the C8DMQCA in DCM is more stable than C7DMQCA. The RDFs binary interactions in the molecules were also computed. The refractive index, the bandgap, absorption, transmission, IR, and Raman spectra were examined in detail. The quinoline derivatives have the allowed direct bandgap. The angle of incidence and refraction, the $(\alpha h\vartheta)^2$ curves, and optical conductivity were investigated and discussed in detail. The results obtained show that the C7DMQCA has desirable optoelectronic properties such as lower optical bandgap, higher refractive index, and optical conductivity than the C8DMQCA.

Acknowledgments The numerical calculations were also partially performed at TUBITAK ULAKBIM, High Performance and Grid Computing Centre (TRUBA resources), Turkey.

Compliance with ethical standards

Conflict of interest The authors declare that they have no conflict of interest.

References

1. Tu Q, Yin Z, Ma Y, Chen S-C, Zheng Q (2018). Dyes Pigments 149:747
2. Xie C, You P, Liu Z, Li L, Yan F (2017). Light Sci Appl 6:e1702
3. Lee W, Choi J, Jung JW (2019). Dyes Pigments 161:283
4. Sio AD, Lienau C (2017). Phys Chem Chem Phys 19:18813
5. Ameen MY, Abhijith T, Susmita D, Ray SK, Reddy VS (2013). Org Electron 14:554
6. Cho MJ, Sim KM, Bae S-R, Choi HO, Kim SY, Chung DS, Park K (2018). Dyes Pigments 149:415
7. Wang JB, Li WL, Chu B, Lee CS, Su ZS, Zhang G, Wu SH, Yan F (2011). Org Electron 12:34
8. Aziz F, Sayyad MH, Sulaiman K, Mailis BY, Karimov KS, Ahmad Z, Sugandi G (2012). Meas Sci Technol 23:014001
9. Murugavelu M, Imran PKM, Sankaran KR, Nagarajan S (2013). Mater Sci Semicond Process 16:461
10. Liu D, Chu Y, Wu X, Huang J (2017). Science China Math 60:977
11. Gillanders RN, Samuel IDW, Turnbull GA (2017). Sensor Actuat B-Chem 245:334
12. Huang Y, Yuan R, Zhou S (2012). J Mater Chem 22:883
13. Huang Y, Fu L, Zou W, Zhang F (2012). New J Chem 36:1080
14. Slodek A, Zych D, Maroń A, Malecki JG, Golba S, Szafraniec-Gorol G, Pajak M (2019). Dyes Pigments 160:604
15. Hamilton R, Smith J, Ogier S, Heeney M, Anthony JE, McCulloch I, Veres J, Bradley DDC, Anthopoulos TD (2009). Adv Mater 21: 1166
16. An TK, Park S-M, Nam S, Hwang J, Yoo S-J, Lee M-J et al (2013). Sci Adv Mater 5:1323
17. Marella A, Tanwar OP, Saha R et al (2013). Saudi Pharm J 21:1
18. Gorka AP, De Dios A, Roepe PD (2013). J Med Chem 56:5231
19. Hisham S, Tajuddin HA, Chee CF, Hasan ZA, Abdullah Z (2019). J Lumin 208:245
20. Rafiee MA, Hadipour NL, N-Manesh H (2004). J Comput Aided Mol Des 18:215
21. Kharb R, Kaur H (2013). Int Res J Pharm 4:63
22. Khan SA, Asiri AM, Al-Thaqafy SH, Aidallah HMF, El-Daly SA (2014). Spectrochim Acta 133:141
23. Sangani CB, Makawana JA, Zhang X, Teraiya SC, Lin I, Zhu HL (2014). Eur J Med Chem 76:549
24. Wang LY, Chen Q-W, Zhai G-H, Wen Z-Y, Zhang Z-X (2007). Dyes Pigments 72:357
25. Mao M, Zhang X, Zhu B, Wang J, Wu G, Yin Y, Song Q (2016). Dyes Pigments 124:72
26. Al-Busafi SN, Suliman FEO, Al-Alawi ZR (2014). Dyes Pigments 103:138
27. Suliman FEO, Al-Busafi SN, Al-Risi M, Al-Badi KN (2012). Dyes Pigments 92:1153
28. Kohn W, Sham LJ (1965). Phys Rev 140:A1133
29. Becke AD (1988). Phys Rev A 38:3098
30. Vosko SH, Vilk L, Nusair M (1980). Can J Phys 58:1200
31. Lee C, Yang W, Parr RG (1988). Phys Rev B 37:785
32. Yanai T, Tew DP, Handy NC (2004). Chem Pys Lett 393:51
33. Foster ME, Wong BM (2012). J Chem Theory Comput 8:2682
34. Kurban M (2018). Optik 172:295
35. M. J. Frisch, G. W. Trucks, H. B. Schlegel, G. E. Scuseria, M. A. Robb, J. R. Cheeseman, G. Scalmani, V. Barone, B. Mennucci, G. A. Petersson, et al., Gaussian 09, Revision B.01; Gaussian, Inc., Wallingford CT, (2009)
36. Roy Dennington TK and JM. Gauss View, Version 5, Semichem Inc, Shawnee Mission KS, 2009
37. Gündüz B, Kurban M (2018). Vib Spectrosc 96(246):46
38. Tauc J, Menth A (1972). J Non-Cryst Solids 569:8
39. Abeles F (1972) Optical properties of solids. North-Holland Publishing Company, London, Amsterdam
40. Tripathy SK (2015). Opt Mater 46:240
41. Lee S, Jeong I, Kim HP, Hwang SY, Kim TJ, Kim YD, Jang J, Kim J (2013). Sol Energy Mater Sol Cells 118:9
42. Adachi S (1999) Optical constants of crystalline and amorphous semiconductors. Kluwer Academic Publishers
43. Pankov JI (1975) Optical Processes in Semiconductors. Dover, New York, p 91